

---

# ChoiceNet: Robust Learning by Revealing Output Correlations

---

Sungjoon Choi Sanghoon Hong Sungbin Lim  
Kakao Brain

{sungjoon.choi, sanghoon.hong, sungbin.lim}@kakaobrain.com

## Abstract

In this paper, we focus on the supervised learning problem with corrupted training data. We assume that the training dataset is generated from a mixture of a target distribution and other unknown distributions. We estimate the quality of each data by revealing the correlation between the generated distribution and the target distribution. To this end, we present a novel framework referred to here as ChoiceNet that can robustly infer the target distribution in the presence of inconsistent data. We demonstrate that the proposed framework is applicable to both classification and regression tasks. ChoiceNet is evaluated in comprehensive experiments, where we show that it constantly outperforms existing baseline methods in the handling of noisy data. Particularly, ChoiceNet is successfully applied to autonomous driving tasks where it learns a safe driving policy from a dataset with mixed qualities. In the classification task, we apply the proposed method to the MNIST and CIFAR-10 datasets and it shows superior performances in terms of robustness to noisy labels.

## 1 Introduction

Training a deep neural network requires immense amounts of training data which are often collected using crowdsourcing methods, such as Amazon’s Mechanical Turk (AMT). However, in practice, the crowd-sourced labels are often noisy [4]. Furthermore, deep neural networks are vulnerable to over-fitting given the noisy training data in that they are capable of memorizing the entire dataset even with inconsistent labels, leading to a poor generalization performance [45].

Assuming that a training dataset is generated from a mixture of a target distribution and other distributions, we address this problem through the principled idea of revealing the correlation between the target distribution and the other distributions. We present a framework for robust learning which is applicable to arbitrary neural network architectures such as convolutional neural networks [20] or recurrent neural networks [11]. We call this framework ChoiceNet.

Throughout this paper, we aim to address the following questions:

1. How can we measure the quality of training data in a principled manner?
2. In the presence of inconsistent outputs, how can we infer the target distribution in a scalable manner?

Traditionally, noisy outputs are handled by modeling additive random distributions, often leading to robust loss functions [19]. However, we argue that these approaches are too restrictive when handling severe outliers or inconsistencies in the datasets. To address the first question, we leverage the concept of a correlation. Precisely, we measure the quality of training data using the correlation between the target distribution and the data generating distribution. However, estimating the correct correlation requires an access to a target distribution, whereas learning the correct target distribution requires knowing the correlation between the distributions to be known, making it a chicken-and-egg problem. To address the second question, we simultaneously estimate the target distribution as well

as the correlation in an end-to-end-manner using stochastic gradient decent methods, in this case Adam [26], to achieve scalability.

The cornerstone of the proposed method is a mixture of correlated density network (MCDN) block. First, we present a Cholesky transform method for sampling the weights of a neural network that enables us to model correlated outputs. We also present an effective regularizer to train ChoiceNet. To the best of our knowledge, this represents the first approach simultaneously to infer the target distribution and the output correlations using a neural network in an end-to-end manner.

Revealing the output correlations was proposed in earlier work [6], in which a multi-task Gaussian process prediction (MTGPP) model is proposed. In particular, MTGPP used correlated Gaussian processes to model multiple tasks by learning a free-form cross-covariance matrix. However, due to the multi-task learning setting, it is not suitable for learning a single target function. In other work [8], a leverage optimization method which optimizes the leverage of each demonstrations is proposed. Unlike to former study [6], the latter [8] focused on inferring a single expert policy by incorporating a sparsity constraint by assuming that the most demonstrations are collected from a skillful consistent expert.

ChoiceNet is initially applied to a synthetic regression task, where we demonstrate its robustness to extreme outliers and ability to distinguish the target distribution and noise distributions. We then apply it to an autonomous driving scenario in which the driving demonstrations are collected from both safe and careless drivers and show that it can robustly learn a safe and stable driving policy. Subsequently, we move on to the classification tasks using the MNIST and CIFAR-10 datasets. We show that the proposed method outperforms existing baseline methods in terms of robustness with regard to the handling of noisy labels.

## 2 Related Work

Recently, robustness in deep learning has been actively studied [14] as deep neural networks are being applied to diverse tasks involving real-world applications such as autonomous driving [33] or medical diagnosis [18] where a simple malfunction can have catastrophic results [1]. Perhaps, the most actively studied area regarding robustness in deep learning is the modeling and defense against adversarial attacks in the input domain [2, 40, 7, 34]. Adversarial examples are intentionally designed inputs that cause incorrect predictions in learned models by adding a small perturbation that is scarcely recognized by humans [17]. While this is a substantially important research direction, we focus on the noise in the outputs, e.g., outliers from different distributions or random labels.

A number of studies [3, 35, 15, 24, 31] deal with the problems which arise when handling noisy labels in the training dataset in that massive datasets such as the ImageNet dataset [13] are often mostly from crowdsourcing and which thus may contain inaccurate and inconsistent labels [4]. To deal with noisy labels, an earlier study [3] proposed an extra layer for the modeling of output noises. Later work [24] extended the aforementioned approach [3] by adding an additional noise adaptation layer with aggressive dropout regularization. A similar method was then proposed [35] which initially estimated the label corruption matrix with a learned classifier and used the corruption matrix to fine-tune the classifier. Other research [23] concentrated on the training of an additional neural network, referred to as MentorNet, which assigns a weight to each instance of training data to supervise the training of a base network, termed StudentNet, to overcome the over-fitting of corrupted training data. On final study of note here [39] analyzed the intrinsic robustness of deep neural network models to massive label noise and empirically showed that a larger batch size with a lower learning rate can be beneficial with regard to the robustness. Motivated by that work [39], we train ChoiceNet with a large batch size and a low learning rate.

Unlike previous methods that only require noisy training datasets, some work [30, 32, 22, 42] require a small number of clean datasets. A gold-loss correction method was also presented [22]; it initially learns a label corruption matrix using a small clean dataset and then uses the corruption matrix to retrain a corrected classifier. A label-cleaning network has also been proposed [42]. It corrects noisy labels in the training dataset by leveraging information from a small clean dataset.

Adding small label noises while training is known to be beneficial to training, as it can be regarded as an effective regularization method [29, 16]. Similar methods have been proposed to tackle noisy outputs. A bootstrapping method [38] which train a neural network with a convex combination of the output of the current network and the noisy target was proposed. Other researchers [43] proposed DisturbLabel, a simple method which randomly replaces a percentage of the labels with incorrect values for each iteration. Mixing both input and output data was also proposed [41, 46]. One study

[46] considered the image recognition problem under label noise and the other [41] focused on a sound recognition problem.

Modeling correlations of output training data has been actively studied in light of Gaussian processes [36]. MTGPP [6] that models the correlations of multiple tasks via Gaussian process regression was also proposed. Due to the multi-task setting, however, [6] is not suitable for robust regression tasks. Other researchers [8] proposed a robust learning from demonstration method using a sparse constrained leverage optimization method which estimates the correlation between training outputs. Unlike the former study [6], the latter above [8] can robustly recover the expert policy function. While our problem setting is similar to the latter study [8], we propose end-to-end learning of both the target distribution and the correlation of each training data, thus offering, a clear advantage in terms of scalability. The aforementioned study [8] also requires the design of a proper kernel structure, which is not suitable for high-dimensional inputs and classification problems.

### 3 ChoiceNet

In this section, we introduce a foundational theory and the model architecture of ChoiceNet. ChoiceNet consists of a base network and a mixture of correlated density network (MCDN) block. Section 3.1 legitimates the reparameterization trick for correlated samples. Subsequently, we present the mechanism of ChoiceNet in Section 3.2 and loss functions for ChoiceNet regarding regression and classification tasks in Section 3.3.

#### 3.1 Reparameterization Trick for Correlated Sampling

We introduce fundamental theorems which lead to *Cholesky transform* for given random variables  $(W, Z)$ . We apply this transform to random matrices  $\mathbf{W}$  and  $\mathbf{Z}$  which carry out weight matrices for prediction and a supplementary role, respectively. Each proof of theorem can be found in the Appendix.

**Theorem 1.** *Let  $W$  and  $Z$  be uncorrelated random variables such that*

$$\begin{cases} \mathbb{E}W = \mu_W, & \mathbb{V}(W) = \sigma_W^2 \\ \mathbb{E}Z = 0, & \mathbb{V}(Z) = \sigma_Z^2 \end{cases} \quad (1)$$

For a given  $-1 \leq \rho \leq 1$ , set

$$\tilde{Z} = \rho \frac{\sigma_Z}{\sigma_W} (W - \mu_W) + \sqrt{1 - \rho^2} Z \quad (2)$$

Then

$$\mathbb{E}\tilde{Z} = 0, \quad \mathbb{V}(\tilde{Z}) = \sigma_Z^2, \quad \text{Corr}(W, \tilde{Z}) = \rho$$

**Theorem 2.** *Assume the same condition in Theorem 1 and define  $\tilde{Z}$  as (2). For given functions  $\varphi : \mathbb{R} \rightarrow \mathbb{R}$  and  $\psi : \mathbb{R} \rightarrow (0, \infty)$ , set  $\tilde{W} := \varphi(\rho) + \psi(\rho)\tilde{Z}$ . Then*

$$\mathbb{E}\tilde{W} = \varphi(\rho), \quad \mathbb{V}(\tilde{W}) = |\psi(\rho)|^2 \sigma_Z^2, \quad \text{Corr}(W, \tilde{W}) = \rho$$

Due to the above theorem, correlation is invariant to mean-translation and variance-dilatation. Now we define the key operation of the MCDN block named *Cholesky Transform*.

**Definition.** For  $-1 < \rho < 1$ , we define Cholesky transform as follows

$$\mathcal{T}_{(w,z)}(\rho, \mu_W, \mu_Z, \sigma_W, \sigma_Z) := \rho \mu_W + \sqrt{1 - \rho^2} \left( \rho \frac{\sigma_Z}{\sigma_W} (w - \mu_W) + \sqrt{1 - \rho^2} z \right) \quad (3)$$

Here  $\mathcal{T}_{(\cdot, \cdot)} : \mathbb{R}^2 \rightarrow \mathbb{R}$  is a function for given parameters  $(\rho, \mu_W, \mu_Z, \sigma_W, \sigma_Z)$ . By plugging random variables  $(W, Z)$  in  $(w, z)$ , we obtain a new random variable  $\mathcal{T}_{(W,Z)}$  correlated with  $W$ . This makes it possible to use the reparametrization trick [27, 28] to learn parameters  $\rho, \mu_W$ , and  $\sigma_W$ . Indeed,  $\mathcal{T}_{(W,Z)} = \rho \mu_W + \sqrt{1 - \rho^2} \tilde{Z}$  according to (2). Thus by applying Theorem 2 to  $\mathcal{T}_{(W,Z)}$  with  $\varphi(\rho) = \rho \mu_W$  and  $\psi(\rho) = \sqrt{1 - \rho^2}$ , we reach the following result.

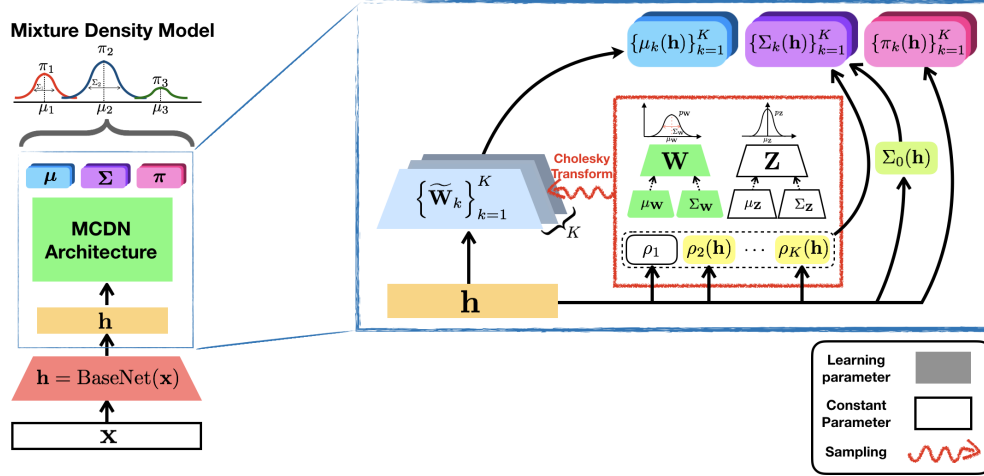


Figure 1: Model Architecture of ChoiceNet

**Corollary.** Under the same conditions in Theorem 1, let

$$\tilde{W} := \mathcal{T}_{(W,Z)}(\rho, \mu_W, \mu_Z, \sigma_W, \sigma_Z)$$

Then

$$\mathbb{E}\tilde{W} = \rho\mu_W, \quad \mathbb{V}(\tilde{W}) = (1 - \rho^2)\sigma_Z^2, \quad \text{Corr}(W, \tilde{W}) = \rho$$

Aforementioned Corollary implies the random variable  $\tilde{W}$  has a correlation  $\rho$  with  $W$ . The following theorem further states that a correlation between random matrices is invariant to an affine transform. This legitimates using Cholesky transform to generate weight matrices  $\{\tilde{W}_k\}_{k=1}^K$  in the MCDN block.

**Theorem 3.** Let  $\rho = (\rho_1, \dots, \rho_K) \in \mathbb{R}^K$ . For  $p \in \{1, 2\}$ , random matrices  $\mathbf{W}^{(p)} \in \mathbb{R}^{K \times Q}$  are given such that for every  $k \in \{1, \dots, K\}$ ,

$$\text{Cov}\left(W_{ki}^{(p)}, W_{kj}^{(p)}\right) = \sigma_p^2 \delta_{ij} \quad (4)$$

and

$$\text{Cov}\left(W_{ki}^{(1)}, W_{kj}^{(2)}\right) = \rho_k \sigma_1 \sigma_2 \delta_{ij} \quad (5)$$

Given  $\mathbf{h} = (h_1, \dots, h_Q) \in \mathbb{R}^Q$ , set  $\mathbf{y}^{(p)} = \mathbf{W}^{(p)}\mathbf{h}$  for each  $p \in \{1, 2\}$ . Then an elementwise correlation between  $\mathbf{y}^{(1)}$  and  $\mathbf{y}^{(2)}$  equals  $\rho$  i.e.

$$\text{Corr}\left(y_k^{(1)}, y_k^{(2)}\right) = \rho_k, \quad \forall k \in \{1, \dots, K\}$$

equivalently,

$$\text{Corr}\left(\mathbf{y}^{(1)}, \mathbf{y}^{(2)}\right) = \rho$$

### 3.2 Model Architecture

In this section, we describe the model architecture and the mechanism of ChoiceNet. In the followings,  $\tau^{-1} > 0$  is a constant indicating expected measurement noise and  $\eta(\cdot) \in (-1, 1)$  is a bounded function, e.g., a hyperbolic tangent.  $\mathbf{W}_{\mathbf{h} \rightarrow \rho}, \mathbf{W}_{\mathbf{h} \rightarrow \pi} \in \mathbb{R}^{K \times Q}$  and  $\mathbf{W}_{\mathbf{h} \rightarrow \Sigma_0} \in \mathbb{R}^{D \times Q}$  where  $Q$  and  $D$  denote the dimensions of a feature vector  $\mathbf{h}$  and output  $\mathbf{y}$ , respectively, and  $K$  is the number of mixtures.  $\rho_{\max}$  is a fixed constant whose value is close to 1.

ChoiceNet is a twofold architecture: (a) a base network and (b) a MCDN block (see Figure 1). A base network extracts features for a given dataset. Then the MCDN block estimates the densities of the data generating distributions through  $(\mu_k, \Sigma_k, \pi_k)_{k=1}^K$ . Contrary to the mixture density network (MDN), during the density estimation process, the MCDN block samples correlated weights using

Cholesky transform. Consequently, the MCDN block is able to generate the correlated mean vectors  $\boldsymbol{\mu}$ . The overall mechanism of ChoiceNet can be elaborated as follows:

$$\begin{aligned}
\text{Modules} &= \begin{cases} \mathbf{h} = \text{BaseNet}(\mathbf{x}) \in \mathbb{R}^Q \\ \boldsymbol{\rho}(\mathbf{h}) = \eta(\mathbf{W}_{\mathbf{h} \rightarrow \boldsymbol{\rho}} \mathbf{h}) \in \mathbb{R}^K = (\rho_1, \rho_2(\mathbf{h}), \dots, \rho_K(\mathbf{h})), \quad \rho_1 = \rho_{\max} \\ \Sigma_0(\mathbf{h}) = \exp(\mathbf{W}_{\mathbf{h} \rightarrow \Sigma_0} \mathbf{h}) \in \mathbb{R}^D \\ \Sigma_k = (1 - \rho_k^2) \Sigma_0(\mathbf{h}) + \tau^{-1} \in \mathbb{R}^D, \quad k \in \{1, \dots, K\} \end{cases} \\
\text{Cholesky Transform} &= \begin{cases} \mathbf{W} \sim \mathcal{N}(\mu_{\mathbf{W}}, \Sigma_{\mathbf{W}}) \in \mathbb{R}^{D \times Q} \\ \mathbf{Z} \sim \mathcal{N}(\mu_{\mathbf{Z}}, \Sigma_{\mathbf{Z}}) \in \mathbb{R}^{D \times Q} \\ \widetilde{\mathbf{W}}_k = \mathcal{T}_{(\mathbf{W}, \mathbf{Z})}(\rho_k(\mathbf{h}), \mu_{\mathbf{W}}, \mu_{\mathbf{Z}}, \Sigma_{\mathbf{W}}, \Sigma_{\mathbf{Z}}) \in \mathbb{R}^{D \times Q}, \quad k \in \{1, \dots, K\} \end{cases} \\
\text{Outputs} &= \begin{cases} \boldsymbol{\mu} = (\mu_1, \dots, \mu_K) = (\widetilde{\mathbf{W}}_1 \mathbf{h}, \dots, \widetilde{\mathbf{W}}_K \mathbf{h}) \in \mathbb{R}^{K \times D} \\ \boldsymbol{\pi} = (\pi_1, \dots, \pi_K) = \text{softmax}(\mathbf{W}_{\mathbf{h} \rightarrow \boldsymbol{\pi}} \mathbf{h}) \in \mathbb{R}^K \\ \boldsymbol{\Sigma} = (\Sigma_1, \dots, \Sigma_K) \in \mathbb{R}^{K \times D} \end{cases}
\end{aligned}$$

By Theorem 3, for each  $k \in \{1, \dots, K\}$

$$\text{Corr}(\mu_k, \mathbf{W}\mathbf{h}) = \text{Corr}(\widetilde{\mathbf{W}}_k \mathbf{h}, \mathbf{W}\mathbf{h}) = (\rho_k, \dots, \rho_k) \in \mathbb{R}^D,$$

and the output density is modeled via correlated mean vectors. Note that both  $\mathbb{V}(\mu_k)$  and  $\Sigma_k$  are minimized, when  $\rho_k \rightarrow \pm 1$ . Furthermore, as we apply Gaussian distributions for Cholesky transform, the influences of uninformative or independent data, whose correlations are close to 0, is attenuated as their variances increase [25].

### 3.3 Training Objectives

Denote a training dataset by  $\mathcal{D} = \{(\mathbf{x}_i, \mathbf{y}_i) : i = 1, \dots, N\}$ . We consider both regression and classification tasks.

**Regression** For the regression task, we employ both  $L_2$ -loss and the standard MDN loss [5, 9, 10];

$$\mathcal{L}(\mathcal{D}) = \frac{1}{N} \sum_{i=1}^N \left[ \lambda_1 \|\mathbf{y}_i - \mu_1(\mathbf{x}_i)\|_2^2 + \lambda_2 \log \left( \sum_{k=1}^K \pi_k(\mathbf{x}_i) \mathcal{N}(\mathbf{y}_i; \mu_k(\mathbf{x}_i), \text{diag}(\Sigma_k(\mathbf{x}_i))) \right) \right] \quad (6)$$

where  $\lambda_1$  and  $\lambda_2$  are hyper-parameters and  $\mathcal{N}(\cdot | \mu, \Sigma)$  is the density of multivariate Gaussian:

$$\mathcal{N}(\mathbf{y}_i; \mu_k(\mathbf{x}_i), \text{diag}(\Sigma_k(\mathbf{x}_i))) = \prod_{d=1}^D \frac{1}{\sqrt{2\pi\Sigma_k^{(d)}}} \exp\left(-\frac{|y_i^{(d)} - \mu_k^{(d)}|^2}{2\Sigma_k^{(d)}}\right)$$

We also add weight decay and the following Kullback-Leibler regularizer to (6)

$$\mathbb{KL}(\bar{\boldsymbol{\rho}} \| \boldsymbol{\pi}) = \sum_{k=1}^K \bar{\rho}_k \log \frac{\bar{\rho}_k}{\pi_k}, \quad \bar{\boldsymbol{\rho}} = \text{softmax}(\boldsymbol{\rho}) \quad (7)$$

The above KL regularizer encourages the mixture components with the strong correlations to have high mixture probabilities. This guidance is useful since ChoiceNet uses the mean vector  $\mu_1(\mathbf{x}_i)$  of the first mixture component at the inference stage.

**Classification** In the classification task, we suppose each  $\mathbf{y}_i$  is a  $D$ -dimensional one-hot vector. Unlike the regression task, (6) is not appropriate for the classification task. We employ the following loss function:

$$\mathcal{L}(\mathcal{D}) = -\frac{1}{N} \sum_{i=1}^N \sum_{k=1}^K \pi_k(\mathbf{x}_i) \left( \langle \text{softmax}(\hat{\mathbf{y}}_k(\mathbf{x}_i)), \mathbf{y}_i \rangle - \lambda_{\text{reg}} \log \left( \sum_{d=1}^D \exp(\hat{y}_k^{(d)}(\mathbf{x}_i)) \right) \right) \quad (8)$$

where  $\lambda_{\text{reg}}$  is a hyper-parameter. Similar to the regression task, we use both (7) and weight decay.

Table 1: RMSE of compared methods on synthetic toy examples

Outliers	ChoiceNet	MDN	MLP	GPR	LGPR	RGPR
0%	0.034	0.028	0.039	<b>0.008</b>	0.022	0.017
20%	0.022	0.087	0.413	0.280	0.206	<b>0.013</b>
40%	<b>0.018</b>	0.565	0.452	0.447	0.439	1.322
60%	<b>0.023</b>	0.645	0.636	0.602	0.579	0.738
80%	<b>0.084</b>	0.778	0.829	0.779	0.777	1.523

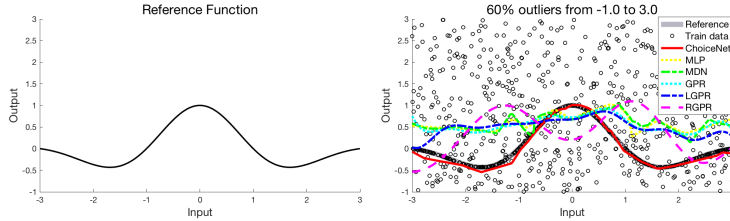


Figure 2: Reference function and fitting results of compared methods on different outlier rates.

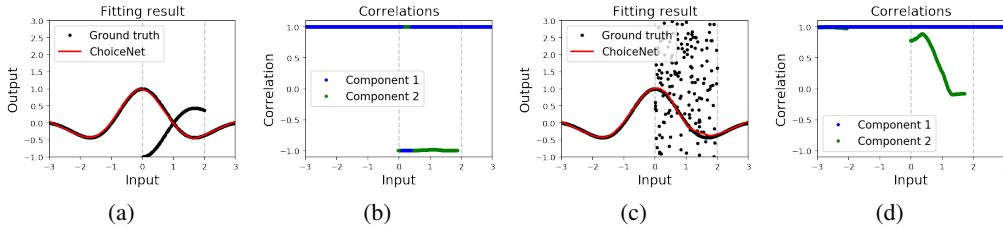


Figure 3: Fitting results on datasets with (a) flipped function and (c) uniform corruptions. Resulting correlations of two components with (b) flipped function and (d) uniform corruptions.

## 4 Experiments

### 4.1 Regression Tasks

We conduct two regression experiments: 1) a synthetic scenario where the training dataset contains outliers sampled from other distributions and 2) a track driving scenario where the driving demonstrations are collected from two different driving modes.

**Synthetic Example** We first apply ChoiceNet to a simple one-dimensional regression problem of fitting  $f(x) = \cos(\frac{\pi}{2}x) \exp(-(\frac{x}{2})^2)$  where  $x \in [-3, +3]$  as shown in Figure 5. ChoiceNet is compared with a naive multilayer perceptron (MLP), a mixture density network (MDN) with five mixtures where all networks have two hidden layers with 32 nodes with a ReLU activation function. Gaussian process regression (GPR) [36], leveraged Gaussian process regression (LGPR) with leverage optimization [8], and robust Gaussian process regression (RGPR) with an infinite Gaussian process mixture model [37] are also compared. For the GP based methods, we use a squared-exponential kernel function and the hyper-parameters are determined using a simple median trick [12]<sup>1</sup>. To evaluate its performance in corrupted datasets, we randomly replace the original target values with outliers whose output values are uniformly sampled from  $-1$  to  $+3$ . We vary the outlier rates from 0% (clean) to 80% (extremely noisy).

Table 1 illustrates the RMSEs (root mean square errors) between the reference target function and the fitted results of ChoiceNet and other compared methods. Given an intact training dataset, all the methods show stable performances in that the RMSEs are all below 0.1. Given training datasets whose outlier rates exceed 40%, however, only ChoiceNet successfully fits the target function whereas the other methods fail as shown in Figure 5.

<sup>1</sup> A median trick selects the length parameter of a kernel function to be the median of all pairwise distances between training data.



Figure 4: Resulting trajectories of compared methods trained with mixed demonstrations. (best viewed in color).

Table 2: Collision rates of compared methods on straight lanes.

Outliers	ChoiceNet	MDN	MLP	GPR	LGPR	RGPR
0%	<b>0%</b>	50.83%	<b>0%</b>	0.83%	4.17%	3.33%
10%	<b>0%</b>	38.33%	<b>0%</b>	2.5%	1.67%	4.17%
20%	<b>0%</b>	41.67%	<b>0%</b>	7.5%	6.67%	10%
30%	<b>0%</b>	66.67%	1.67%	4.17%	1.67%	7.5%
40%	<b>0.83%</b>	35%	3.33%	6.67%	6.67%	24.17%

Table 3: Root mean square lane deviation distances (m) of compared methods on straight lanes.

Outliers	ChoiceNet	MDN	MLP	GPR	LGPR	RGPR
0%	0.314	0.723	<b>0.300</b>	0.356	0.349	0.424
10%	<b>0.352</b>	0.387	0.438	0.401	0.446	0.673
20%	<b>0.349</b>	0.410	0.513	0.418	0.419	0.725
30%	<b>0.368</b>	<b>0.368</b>	0.499	0.455	0.476	0.740
40%	<b>0.370</b>	0.574	0.453	0.453	0.453	0.636

To further inspect whether ChoiceNet can distinguish between the target distribution and noise distributions, we train ChoiceNet on two datasets. In particular, we use the same target function and replace 50% of the output values whose input values are within 0 to 2 using two different corruptions: one uniformly sampled from  $-1$  to 3 and the other from a flipped target function. For this experiment, we set  $K = 2$  for better visualization. As shown in Figure 3(a) and 3(c), ChoiceNet successfully fits the target function. The correlations of the second component decrease as outliers are introduced as shown in Figure 3(b) and 3(d). Surprisingly, when the target and noise distribution are negatively correlated (the flipped function case), the correlations of the second component become  $-1$  as depicted in Figure 3(b). Contrarily, for the uniform corruption case, the correlations of the second component are within 0 and 1. We argue that this clearly shows the capability of ChoiceNet to distinguish the target distribution from noisy distributions.

**Autonomous Driving Experiment** In this experiment, we apply ChoiceNet to a autonomous driving scenario in a simulated environment. In particular, the tested methods are asked to learn the policy from driving demonstrations collected from both safe and careless driving modes. We use the same set of methods used for the previous task. The policy function is defined as a mapping between four dimensional input features consist of three frontal distances to left, center, and right lanes and lane deviation distance from the center of the lane to the desired heading. Once the desired heading is computed, the angular velocity of a car is computed by  $10 * (\theta_{\text{desired}} - \theta_{\text{current}})$  and the directional velocity is fixed to  $10m/s$ . The driving demonstrations are collected from keyboard inputs by human users. The objective of this experiment is to assess its performance on a training set generated from two different distributions. We would like to note that this task does not have a reference target function in that all demonstrations are collected manually. Hence, we evaluated the performances of the compared methods by running the trained policies on a straight track by randomly deploying static cars.

Table 2 and Table 3 indicate collision rates and RMS lane deviation distances of the tested methods, respectively, where the statistics are computed from 50 independent runs on the straight lane by randomly placing static cars as shown in Figure 7. ChoiceNet clearly outperforms compared methods in terms of both safety (low collision rates) and stability (low RMS lane deviation distances).

## 4.2 Classification Tasks

We conduct classification experiments on the MNIST and CIFAR-10 datasets to evaluate the performance of ChoiceNet on corrupted labels. To generate noisy datasets, we follow the setting in [46] which randomly shuffles a percentage of the labels in the dataset<sup>2</sup>. We vary the corruption probabilities from 50% to 95% for the MNIST dataset and from 20% to 80% for the CIFAR-10 dataset and compare median accuracies after five runs for each configuration.

For the MNIST experiments, we construct two networks: a network with two residual blocks [21] with  $3 \times 3 \times 64$  convolutional layers followed by a fully-connected layer with 256 output neurons (ConvNet) and a network with the same two residual blocks followed by a MCDN block (ChoiceNet). We train each network for 50 epochs with a fixed learning rate of  $1e - 5$ .

For the CIFAR experiments, we adopt WideResNet (WRN) [44] with 22 layers and a widening factor of 4. To construct ChoiceNet, we replace the last layer of WideResNet with a MCDN block. We set  $K = 3$ ,  $\rho_{\max} = 0.95$ ,  $\lambda_{\text{reg}} = 0.0001$ , and  $\rho_k, \pi_k, \Sigma_0$  modules consist of two fully connected layers with 64 hidden units and a ReLU activation function. We train each network for 300 epochs with a minibatch size of 256. We begin with a learning rate of 0.1, and it decays by 1/10 after 150 and 225 epochs. We apply random horizontal flip and random crop with 4-pixel-padding and use a weight decay of 0.0001 for the baseline network as [21]. However, to train ChoiceNet, we reduce the weight decay rate to  $1e - 6$  and apply gradient clipping at 1.0. We also lower the learning rate to 0.001 for the first epoch to stabilize training.

On both MNIST and CIFAR-10 experiments, we also compare ChoiceNet with Mixup [46] which, to the best of our knowledge, shows the state-of-the-art performance on noisy labels. We set the parameter  $\alpha$  of Mixup to be 32 for the baseline network as suggested in the original paper. For ChoiceNet, we set  $\alpha$  to be 1.

Table 4: Test accuracies on the MNIST datasets with corrupted labels.

Corruption $p$	Configuration	Best	Last
50%	ConvNet	95.4	89.5
	ConvNet+Mixup	97.2	96.8
	ChoiceNet	<b>99.2</b>	<b>99.2</b>
80%	ConvNet	86.3	76.9
	ConvNet+Mixup	87.2	87.2
	ChoiceNet	<b>98.2</b>	<b>97.6</b>
90%	ConvNet	76.1	69.8
	ConvNet+Mixup	74.7	74.7
	ChoiceNet	<b>94.7</b>	<b>89.0</b>
95%	ConvNet	72.5	64.4
	ConvNet+Mixup	69.2	68.2
	ChoiceNet	<b>88.5</b>	<b>80.0</b>

Table 5: Test accuracies on the CIFAR-10 datasets with corrupted labels

Corruption $p$	Configuration	Best	Last
20%	WRN (WideResNet)	88.5	85.3
	CN ChoiceNet)	90.7	90.3
	WRN + Mixup	<b>92.9</b>	<b>92.3</b>
	CN + Mixup	92.5	<b>92.3</b>
50%	WRN	79.7	59.3
	CN	85.9	84.6
	WRN + Mixup	87.3	83.1
	CN + Mixup	<b>88.4</b>	<b>87.9</b>
80%	WRN	67.8	27.4
	CN	69.8	65.2
	WRN + Mixup	72.1	62.9
	CN + Mixup	<b>76.1</b>	<b>75.4</b>

The classification results of the MNIST dataset and the CIFAR dataset are shown in Table 7 and Table 5, respectively. In the MNIST experiments, ChoiceNet consistently outperforms ConvNet and ConvNet+Mixup by a significant margin, and the difference between the accuracies of ChoiceNet and the others becomes more clear as the corruption probability increases. Particularly, the best test accuracy of ChoiceNet reaches 94% even when 90% of the training labels are randomly shuffled.

In the CIFAR-10 experiments, ChoiceNet outperforms WideResNet and achieves its accuracy over 60% even when 80% of the labels are shuffled whereas the accuracy of WideResNet drops below 30%. When we inspect the training accuracies on the 80%-shuffled set, WideResNet tends to overfit (memorize) to noisy labels and shows 99.8% train accuracy. On the contrary, ChoiceNet shows 37.6%. Detailed learning curves can be found in the Appendix. When trained with Mixup, both

<sup>2</sup>In the corrupted label setting, for a given corruption probability  $p$ , the expected ratio of correct labels is  $(1 - p) + p \times 1/(\text{number of classes})$ . Additional experiments of replacing the percentage of labels to a random labels and a fixed label can be found in the Appendix.

networks become robust to noisy labels to some extent. However, the results of the two networks still show significant differences except for the 20% corrupted experiments on which both of them show similar accuracies. Interestingly, when ChoiceNet and Mixup are combined, it achieves a high accuracy of 75% even on the 80% shuffled dataset. We also note that ChoiceNet (without Mixup) outperforms WideResNet+Mixup when the corruption ratio is over 50% on the last accuracies.

## 5 Conclusion

In this paper, we have presented ChoiceNet that can robustly learn a target distribution given noisy training data. The keystone of ChoiceNet is the mixture of correlated density network block which can estimate the densities of data distributions using a set of correlated mean functions. We have demonstrated that ChoiceNet can robustly infer the target distribution on corrupted training data in the following tasks; regression with synthetic data, autonomous driving, and MNIST and CIFAR-10 image classification tasks. Our experiments verify that ChoiceNet outperforms existing methods in the handling of noisy data.

Selecting proper hyper-parameters including the optimal number of mixture components is a compelling topic for the practical usage of ChoiceNet. Furthermore, one can use ChoiceNet for active learning by evaluating the quality of each training data using through the lens of correlations. We leave these as important questions for future work.

## References

- [1] AP and REUTERS. Tesla working on 'improvements' to its autopilot radar changes after model s owner became the first self-driving fatality., June 2016. URL <https://goo.gl/XkzzQd>.
- [2] A. M. Aung, Y. Fadila, R. Gondokaryono, and L. Gonzalez. Building robust deep neural networks for road sign detection. *arXiv preprint arXiv:1712.09327*, 2017.
- [3] A. J. Bekker and J. Goldberger. Training deep neural-networks based on unreliable labels. In *Proc. of IEEE International Conference on Acoustics, Speech and Signal Processing*, pages 2682–2686. IEEE, 2016.
- [4] W. Bi, L. Wang, J. T. Kwok, and Z. Tu. Learning to predict from crowdsourced data. In *UAI*, pages 82–91, 2014.
- [5] C. M. Bishop. Mixture density networks. 1994.
- [6] E. V. Bonilla, K. M. Chai, and C. Williams. Multi-task gaussian process prediction. In *Proc. of the Advances in Neural Information Processing Systems*, pages 153–160, 2008.
- [7] N. Carlini and D. Wagner. Towards evaluating the robustness of neural networks. In *IEEE Symposium on Security and Privacy*, pages 39–57. IEEE, 2017.
- [8] S. Choi, K. Lee, and S. Oh. Robust learning from demonstration using leveraged Gaussian processes and sparse constrained optimization. In *Proc. of the IEEE International Conference on Robotics and Automation (ICRA)*. IEEE, May 2016.
- [9] S. Choi, K. Lee, S. Lim, and S. Oh. Uncertainty-aware learning from demonstration using mixture density networks with sampling-free variance modeling. *arXiv preprint arXiv:1709.02249*, 2017.
- [10] M. B. Christopher. *PATTERN RECOGNITION AND MACHINE LEARNING*. Springer-Verlag New York, 2016.
- [11] J. Chung, C. Gulcehre, K. Cho, and Y. Bengio. Empirical evaluation of gated recurrent neural networks on sequence modeling. *arXiv preprint arXiv:1412.3555*, 2014.
- [12] B. Dai, B. Xie, N. He, Y. Liang, A. Raj, M.-F. F. Balcan, and L. Song. Scalable kernel methods via doubly stochastic gradients. In *Proc. of the Advances in Neural Information Processing Systems*, pages 3041–3049, 2014.
- [13] J. Deng, W. Dong, R. Socher, L.-J. Li, K. Li, and L. Fei-Fei. Imagenet: A large-scale hierarchical image database. In *Proc. of IEEE Conference on Computer Vision and Pattern Recognition*, pages 248–255. IEEE, 2009.
- [14] A. Fawzi, S. M. M. Dezfouli, and P. Frossard. A geometric perspective on the robustness of deep networks. *IEEE Signal Processing Magazine*, 2017.
- [15] J. Goldberger and E. Ben-Reuven. Training deep neural-networks using a noise adaptation layer. In *Proc. of International Conference on Learning Representations*, 2017.
- [16] I. Goodfellow, Y. Bengio, A. Courville, and Y. Bengio. *Deep learning*, volume 1. MIT press Cambridge, 2016.
- [17] I. J. Goodfellow, J. Shlens, and C. Szegedy. Explaining and harnessing adversarial examples. *arXiv preprint arXiv:1412.6572*, 2014.
- [18] V. Gulshan, L. Peng, M. Coram, M. C. Stumpe, D. Wu, A. Narayanaswamy, S. Venugopalan, K. Widner, T. Madams, J. Cuadros, et al. Development and validation of a deep learning algorithm for detection of diabetic retinopathy in retinal fundus photographs. *Journal of the American Medical Association*, 316(22): 2402–2410, 2016.
- [19] F. R. Hampel, E. M. Ronchetti, P. J. Rousseeuw, and W. A. Stahel. *Robust statistics: the approach based on influence functions*, volume 196. John Wiley & Sons, 2011.
- [20] K. He, X. Zhang, S. Ren, and J. Sun. Deep residual learning for image recognition. In *Proc. of the IEEE conference on Computer Vision and Pattern Recognition*, pages 770–778, 2016.
- [21] K. He, X. Zhang, S. Ren, and J. Sun. Deep residual learning for image recognition. In *Proceedings of the IEEE conference on computer vision and pattern recognition*, pages 770–778, 2016.
- [22] D. Hendrycks, M. Mazeika, D. Wilson, and K. Gimpel. Using trusted data to train deep networks on labels corrupted by severe noise. *arXiv preprint arXiv:1802.05300*, 2018.

- [23] L. Jiang, Z. Zhou, T. Leung, L.-J. Li, and L. Fei-Fei. Mentornet: Regularizing very deep neural networks on corrupted labels. *arXiv preprint arXiv:1712.05055*, 2017.
- [24] I. Jindal, M. Nokleby, and X. Chen. Learning deep networks from noisy labels with dropout regularization. In *Proc. of IEEE International Conference on Data Mining*, pages 967–972. IEEE, 2016.
- [25] A. Kendall and Y. Gal. What uncertainties do we need in bayesian deep learning for computer vision? In *Advances in Neural Information Processing Systems*, pages 5580–5590, 2017.
- [26] D. Kingma and J. Ba. Adam: A method for stochastic optimization. *arXiv preprint arXiv:1412.6980*, 2014.
- [27] D. P. Kingma. Variational inference & deep learning: A new synthesis. *University of Amsterdam*, 2017.
- [28] D. P. Kingma and M. Welling. Auto-encoding variational bayes. *arXiv preprint arXiv:1312.6114*, 2013.
- [29] D.-H. Lee. Pseudo-label: The simple and efficient semi-supervised learning method for deep neural networks. In *Workshop on Challenges in Representation Learning, ICML*, volume 3, page 2, 2013.
- [30] Y. Li, J. Yang, Y. Song, L. Cao, J. Luo, and J. Li. Learning from noisy labels with distillation. *arXiv preprint arXiv:1703.02391*, 2017.
- [31] X. Liu, S. Li, M. Kan, S. Shan, and X. Chen. Self-error-correcting convolutional neural network for learning with noisy labels. In *Proc. of IEEE International Conference on Automatic Face & Gesture Recognition*, pages 111–117. IEEE, 2017.
- [32] E. Malach and S. Shalev-Shwartz. Decoupling" when to update" from" how to update". In *Advances in Neural Information Processing Systems*, pages 961–971, 2017.
- [33] B. Paden, M. Čáp, S. Z. Yong, D. Yershov, and E. Frazzoli. A survey of motion planning and control techniques for self-driving urban vehicles. *IEEE Transactions on Intelligent Vehicles*, 1(1):33–55, 2016.
- [34] N. Papernot, P. McDaniel, S. Jha, M. Fredrikson, Z. B. Celik, and A. Swami. The limitations of deep learning in adversarial settings. In *IEEE European Symposium on Security and Privacy*, pages 372–387. IEEE, 2016.
- [35] G. Patrini, A. Rozza, A. K. Menon, R. Nock, and L. Qu. Making deep neural networks robust to label noise: a loss correction approach. In *Proc. of the Conference on Computer Vision and Pattern Recognition*, volume 1050, page 22, 2017.
- [36] C. E. Rasmussen. Gaussian processes for machine learning. 2006.
- [37] C. E. Rasmussen and Z. Ghahramani. Infinite mixtures of gaussian process experts. In *Advances in Neural Information Processing Systems*, pages 881–888, 2002.
- [38] S. Reed, H. Lee, D. Anguelov, C. Szegedy, D. Erhan, and A. Rabinovich. Training deep neural networks on noisy labels with bootstrapping. *arXiv preprint arXiv:1412.6596*, 2014.
- [39] D. Rolnick, A. Veit, S. Belongie, and N. Shavit. Deep learning is robust to massive label noise. *arXiv preprint arXiv:1705.10694*, 2017.
- [40] A. Sinha, H. Namkoong, and J. Duchi. Certifiable distributional robustness with principled adversarial training. *arXiv preprint arXiv:1710.10571*, 2017.
- [41] Y. Tokozume, Y. Ushiku, and T. Harada. Proc. of international conference on learning representations. 2018.
- [42] A. Veit, N. Alldrin, G. Chechik, I. Krasin, A. Gupta, and S. Belongie. Learning from noisy large-scale datasets with minimal supervision. In *Conference on Computer Vision and Pattern Recognition*, 2017.
- [43] L. Xie, J. Wang, Z. Wei, M. Wang, and Q. Tian. Disturblabel: Regularizing cnn on the loss layer. In *Proc. of the IEEE Conference on Computer Vision and Pattern Recognition*, pages 4753–4762, 2016.
- [44] S. Zagoruyko and N. Komodakis. Wide residual networks. In *BMVC*, 2016.
- [45] C. Zhang, S. Bengio, M. Hardt, B. Recht, and O. Vinyals. Understanding deep learning requires rethinking generalization. In *Proc. of International Conference on Learning Representations*, 2016.
- [46] H. Zhang, M. Cisse, Y. N. Dauphin, and D. Lopez-Paz. mixup: Beyond empirical risk minimization. In *Proc. of International Conference on Learning Representations*, 2017.

In this appendix, we provide full proofs of theorems. We also elaborate the details of conducted experiments with additional illustrative figures and results. Particularly, we show additional classification experiments with the MNIST dataset on different noise configurations.

## A Proof of Theorems in Section 3.1

**Theorem 1.** Let  $W$  and  $Z$  be uncorrelated random variables such that

$$\begin{cases} \mathbb{E}W = \mu_W, & \mathbb{V}(W) = \sigma_W^2 \\ \mathbb{E}Z = 0, & \mathbb{V}(Z) = \sigma_Z^2 \end{cases} \quad (1)$$

For a given  $-1 \leq \rho \leq 1$ , set

$$\tilde{Z} = \rho \frac{\sigma_Z}{\sigma_W} (W - \mu_W) + \sqrt{1 - \rho^2} Z \quad (2)$$

Then

$$\mathbb{E}\tilde{Z} = 0, \quad \mathbb{V}(\tilde{Z}) = \sigma_Z^2, \quad \text{Corr}(W, \tilde{Z}) = \rho$$

*Proof of Theorem 1.* Since  $W$  and  $Z$  are uncorrelated, we have

$$\mathbb{E}[(W - \mu_W)Z] = \mathbb{E}(W - \mu_W)\mathbb{E}Z = 0 \quad (9)$$

By (1), we directly obtain

$$\mathbb{E}\tilde{Z} = \rho \frac{\sigma_Z}{\sigma_W} (\mathbb{E}W - \mu_W) + \mathbb{E}Z = 0$$

Also, by (1) and (9),

$$\begin{aligned} \mathbb{V}(\tilde{Z}) &= \mathbb{E}|\tilde{Z}|^2 = \rho^2 \left( \frac{\sigma_Z}{\sigma_W} \right)^2 \mathbb{V}(W) + \mathbb{V}(Z) + 2\rho \frac{\sigma_Z}{\sigma_W} \underbrace{\mathbb{E}[(W - \mu_W)Z]}_{=0} \\ &= \rho^2 \frac{\sigma_Z^2}{\sigma_W^2} \sigma_W^2 + (1 - \rho^2) \sigma_Z^2 = \sigma_Z^2 \end{aligned}$$

Similarly,

$$\begin{aligned} \text{Cov}(W, \tilde{Z}) &= \mathbb{E}[(W - \mu_W)\tilde{Z}] \\ &= \mathbb{E}\left[(W - \mu_W)\rho \frac{\sigma_Z}{\sigma_W} (W - \mu_W)\right] + \underbrace{\mathbb{E}[(W - \mu_W)Z]}_{=0} \\ &= \rho \frac{\sigma_Z}{\sigma_W} \mathbb{V}(W) = \rho \sigma_Z \sigma_W \end{aligned}$$

Therefore

$$\text{Corr}(W, \tilde{Z}) = \frac{\text{Cov}(W, \tilde{Z})}{\sqrt{\mathbb{V}(W)}\sqrt{\mathbb{V}(\tilde{Z})}} = \frac{\rho \sigma_W \sigma_Z}{\sigma_W \sigma_Z} = \rho$$

The theorem is proved.  $\square$

**Theorem 2.** Assume the same condition in Theorem 1 and define  $\tilde{Z}$  as (2). For given functions  $\varphi : \mathbb{R} \rightarrow \mathbb{R}$  and  $\psi : \mathbb{R} \rightarrow (0, \infty)$ , set  $\tilde{W} := \varphi(\rho) + \psi(\rho)\tilde{Z}$ . Then

$$\mathbb{E}\tilde{W} = \varphi(\rho), \quad \mathbb{V}(\tilde{W}) = |\psi(\rho)|^2 \sigma_Z^2, \quad \text{Corr}(W, \tilde{W}) = \rho$$

*Proof of Theorem 2.* Note that

$$\begin{aligned} \mu_{\tilde{W}} &= \varphi(\rho) + \psi(\rho)\mu_{\tilde{Z}} = \varphi(\rho) \\ \sigma_{\tilde{W}}^2 &= |\psi(\rho)|^2 \mathbb{E}(\tilde{Z} - \mu_{\tilde{Z}})^2 = \psi^2(\rho)\sigma_Z^2 \end{aligned}$$

Therefore, by Theorem 1

$$\begin{aligned} \mathbb{E}[(W - \mu_W)(\tilde{W} - \mu_{\tilde{W}})] &= \psi(\rho)\mathbb{E}[(W - \mu_W)(\tilde{Z} - \mu_{\tilde{Z}})] \\ &= \rho\psi(\rho)\sigma_W\sigma_Z \end{aligned}$$

Hence

$$\text{Corr}(W, \tilde{W}) = \frac{\mathbb{E}[(W - \mu_W)(\tilde{W} - \mu_{\tilde{W}})]}{\sigma_W \sigma_{\tilde{W}}} = \frac{\rho\psi(\rho)\sigma_W\sigma_Z}{\psi(\rho)\sigma_W\sigma_Z} = \rho$$

The theorem is proved.  $\square$

**Theorem 3.** Let  $\boldsymbol{\rho} = (\rho_1, \dots, \rho_K) \in \mathbb{R}^K$ . For  $p \in \{1, 2\}$ , random matrices  $\mathbf{W}^{(p)} \in \mathbb{R}^{K \times Q}$  are given such that for every  $k \in \{1, \dots, K\}$ ,

$$\text{Cov}\left(W_{ki}^{(p)}, W_{kj}^{(p)}\right) = \sigma_p^2 \delta_{ij} \quad (4)$$

and

$$\text{Cov}\left(W_{ki}^{(1)}, W_{kj}^{(2)}\right) = \rho_k \sigma_1 \sigma_2 \delta_{ij} \quad (5)$$

Given  $\mathbf{h} = (h_1, \dots, h_Q) \in \mathbb{R}^Q$ , set  $\mathbf{y}^{(p)} = \mathbf{W}^{(p)}\mathbf{h}$  for each  $p \in \{1, 2\}$ . Then an elementwise correlation between  $\mathbf{y}^{(1)}$  and  $\mathbf{y}^{(2)}$  equals  $\boldsymbol{\rho}$  i.e.

$$\text{Corr}\left(y_k^{(1)}, y_k^{(2)}\right) = \rho_k, \quad \forall k \in \{1, \dots, K\}$$

equivalently,

$$\text{Corr}\left(\mathbf{y}^{(1)}, \mathbf{y}^{(2)}\right) = \boldsymbol{\rho}$$

*Proof of Theorem 3.* First we prove that for  $p \in \{1, 2\}$  and  $k \in \{1, \dots, K\}$

$$\mathbb{V}\left(y_k^{(p)}\right) = \sigma_p^2 \|\mathbf{h}\|^2 \quad (10)$$

Note that

$$\begin{aligned} \mathbb{V}\left(y_k^{(p)}\right) &= \mathbb{E}\left[\left(\sum_{i=1}^Q W_{ki}^{(p)} h_i - \mathbb{E}\left[\sum_{i=1}^Q W_{ki}^{(p)} h_i\right]\right)^2\right] \\ &= \mathbb{E}\left[\left(\sum_{i=1}^Q \left(W_{ki}^{(p)} - \mathbb{E}W_{ki}^{(p)}\right) h_i\right)^2\right] \\ &= \mathbb{E}\left[\sum_{i,j} \left(W_{ki}^{(p)} - \mathbb{E}W_{ki}^{(p)}\right) \left(W_{kj}^{(p)} - \mathbb{E}W_{kj}^{(p)}\right) h_i h_j\right] \\ &= \sum_{i,j} \text{Cov}\left(W_{ki}^{(p)}, W_{kj}^{(p)}\right) h_i h_j \end{aligned}$$

By (4),

$$\mathbb{V}\left(y_k^{(p)}\right) = \sum_{i,j} \text{Cov}\left(W_{ki}^{(p)}, W_{kj}^{(p)}\right) h_i h_j = \sum_{i,j} \sigma_p^2 h_i h_j \delta_{ij} = \sum_{i=1}^Q \sigma_p^2 h_i^2 = \sigma_p^2 \|\mathbf{h}\|^2$$

so (10) is proved. Next we prove

$$\text{Cov}\left(y_k^{(1)}, y_k^{(2)}\right) = \rho_k \sigma_1 \sigma_2 \|\mathbf{h}\|^2 \quad (11)$$

Observe that

$$\begin{aligned} \text{Cov}\left(y_k^{(1)}, y_k^{(2)}\right) &= \mathbb{E}\left[\left(y_k^{(1)} - \mathbb{E}y_k^{(1)}\right) \left(y_k^{(2)} - \mathbb{E}y_k^{(2)}\right)\right] \\ &= \mathbb{E}\left[\left(\sum_{i=1}^Q W_{ki}^{(1)} h_i - \mathbb{E}\left[\sum_{i=1}^Q W_{ki}^{(1)} h_i\right]\right) \left(\sum_{j=1}^Q W_{kj}^{(2)} h_j - \mathbb{E}\left[\sum_{j=1}^Q W_{kj}^{(2)} h_j\right]\right)\right] \\ &= \mathbb{E}\left[\sum_{i,j} \left(W_{ki}^{(1)} - \mathbb{E}W_{ki}^{(1)}\right) \left(W_{kj}^{(2)} - \mathbb{E}W_{kj}^{(2)}\right) h_i h_j\right] \\ &= \sum_{i,j} \text{Cov}\left(W_{ki}^{(1)}, W_{kj}^{(2)}\right) h_i h_j \end{aligned}$$

Similarly,

$$\text{Cov}\left(y_k^{(1)}, y_k^{(2)}\right) = \sum_{i,j} \text{Cov}\left(W_{ki}^{(1)}, W_{kj}^{(2)}\right) h_i h_j = \sum_{i,j} \rho_k \sigma_1 \sigma_2 h_i h_j \delta_{ij} = \rho_k \sigma_1 \sigma_2 \|\mathbf{h}\|^2$$

Hence (11) is proved. Therefore by (10) and (11)

$$\text{Corr}\left(y_k^{(1)}, y_k^{(2)}\right) = \frac{\text{Cov}\left(y_k^{(1)}, y_k^{(2)}\right)}{\sqrt{\mathbb{V}\left(y_k^{(1)}\right)} \sqrt{\mathbb{V}\left(y_k^{(2)}\right)}} = \frac{\rho_k \sigma_1 \sigma_2 \|\mathbf{h}\|^2}{\sqrt{\sigma_1^2 \|\mathbf{h}\|^2} \sqrt{\sigma_2^2 \|\mathbf{h}\|^2}} = \rho_k$$

The theorem is proved.  $\square$

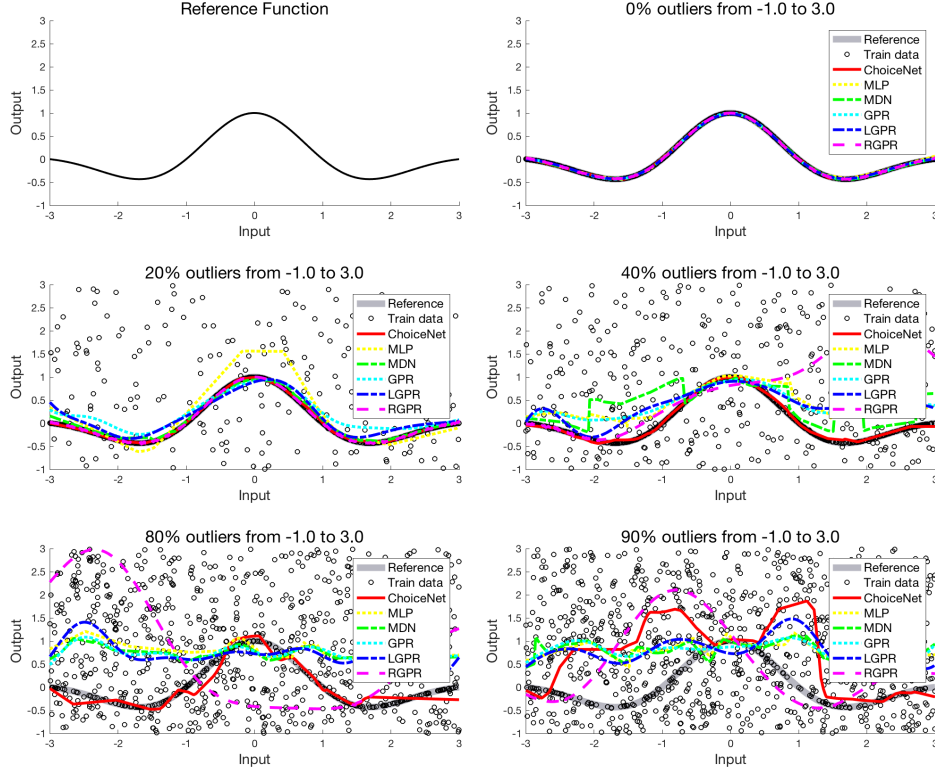


Figure 5: Reference function and fitting results of compared methods on different outlier rates, 0%, 20%, 40%, 80%, and 90%.

*Remark.* Recall the definition of Cholesky transform: for  $-1 < \rho < 1$

$$\mathcal{T}_{(w,z)}(\rho, \mu_W, \mu_Z, \sigma_W, \sigma_Z) := \rho\mu_W + \sqrt{1-\rho^2} \left( \rho \frac{\sigma_Z}{\sigma_W} (w - \mu_W) + \sqrt{1-\rho^2} z \right) \quad (12)$$

Note that we do not assume  $W$  and  $Z$  should follow typical distributions. Hence every above theorems hold for general class of random variables. Additionally, by Theorem 2 and (12),  $\tilde{W}$  has the following  $\rho$ -dependent behaviors;

$$\mathbb{E}\tilde{W} \rightarrow \begin{cases} \mu_W & : \rho \rightarrow 1 \\ 0 & : \rho \rightarrow 0 \\ -\mu_W & : \rho \rightarrow -1 \end{cases}, \quad \mathbb{V}(\tilde{W}) \rightarrow \begin{cases} 0 & : \rho \rightarrow \pm 1 \\ \sigma_Z^2 & : \rho \rightarrow 0 \end{cases}$$

Thus strongly correlated weights  $\tilde{W}$  i.e.  $\rho \approx 1$ , provide prediction with confidence while uncorrelated weights encompass uncertainty. These different behaviors of weights perform regularization and preclude over-fitting caused by bad data since uncorrelated and negative correlated weights absorb vague and outlier pattern, respectively.

## B Experiments

### B.1 Regression Tasks

#### B.1.1 Synthetic Example

We provide more fitting results for the synthetic example in Figure 5. Given an intact dataset, all compared methods robustly fit the given training data. However, other methods fail to correctly fit the underlying target function given corrupted data. When the outlier rate exceeds 90% all tested methods fail to fit.

#### B.1.2 Autonomous Driving Experiment

Here, we describe the features used for the autonomous driving experiments. As shown in the manuscript, we use a four dimensional feature, a lane deviation distance of an ego car, and three frontal distances to the closest

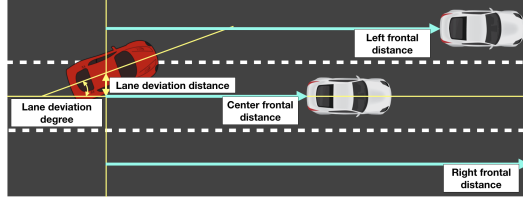


Figure 6: Descriptions of the features of an ego red car used in autonomous driving experiments.

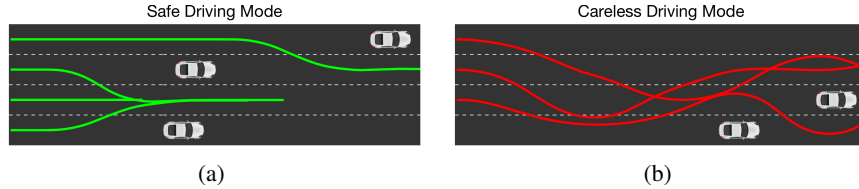


Figure 7: Manually collected trajectories of (a) safe driving mode and (b) careless driving mode. (best viewed in color).

car at left, center, and right lanes as shown in Figure 6. We upperbound the frontal distance to  $40m$ . Figure 7(a) and 7(b) illustrate manually collected trajectories of a safe driving mode and a careless driving mode.

## B.2 Classification Tasks

### B.2.1 MNIST

Here, we present additional experimental results using the MNIST dataset on following three different scenarios:

1. Biased label experiments where we randomly assign the percentage of the training labels to label 0.
2. Random shuffle experiments where we randomly replace the percentage of the training labels from the uniform multinomial distribution.
3. Random permutation experiments where we replace the percentage of the labels based on the label permutation matrix where we follow the random permutation in [38].

The best and final accuracies on the intact test dataset for biased label experiments are shown in Table 6. In all corruption rates, ChoiceNet achieves the best performance compared to two baseline methods. The learning curves of the biased label experiments are depicted in Figure 8. Particularly, we observe unstable learning curves regarding the test accuracies of ConvNet and Mixup. As training accuracies of such methods show stable learning behaviors, this can be interpreted as the networks are simply memorizing noisy labels. In the contrary, the learning curves of ChoiceNet show stable behaviors which clearly indicates the robustness of the proposed method.

The experimental results and learning curves of the random shuffle experiments are shown in Table 7 and Figure 9. The convolutional neural networks trained with Mixup show robust learning behaviors when 80% of the training labels are uniformly shuffled. However, given an extremely noisy dataset (90% and 95%), the test accuracies of baseline methods decrease as the number of epochs increases. ChoiceNet shows outstanding robustness to the noisy dataset in that the test accuracies do not drop even after 50 epochs for the cases where the corruption rates are below 90%. For the 95% case, however, over-fitting is occurred in all methods.

Table 8 and Figure 10 illustrate the results of the random permutation experiments. Specifically, we change the labels of randomly selected training data using a permutation rule:  $(0, 1, 2, 3, 4, 5, 6, 7, 8, 9) \rightarrow (7, 9, 0, 4, 2, 1, 3, 5, 6, 8)$  following [38]. We argue that this setting is more arduous than the random shuffle case in that we are intentionally changing the labels based on predefined permutation rules.

### B.2.2 CIFAR-10

Here, we present detailed learning curves of the CIFAR-10 experiments while varying the noise level from 20% to 80% following the configurations in [46] in Figure 11.

Table 6: Test accuracies on the MNIST dataset with biased label.

Corruption $p$	Configuration	Best	Last
25%	ConvNet	95.4	89.5
	ConvNet+Mixup	97.2	96.8
	ChoiceNet	<b>99.2</b>	<b>99.2</b>
40%	ConvNet	86.3	76.9
	ConvNet+Mixup	87.2	87.2
	ChoiceNet	<b>98.2</b>	<b>97.6</b>
45%	ConvNet	76.1	69.8
	ConvNet+Mixup	74.7	74.7
	ChoiceNet	<b>94.7</b>	<b>89.0</b>
47%	ConvNet	72.5	64.4
	ConvNet+Mixup	69.2	68.2
	ChoiceNet	<b>88.5</b>	<b>80.0</b>

Table 7: Test accuracies on the MNIST dataset with corrupted label.

Corruption $p$	Configuration	Best	Last
50%	ConvNet	97.1	95.9
	ConvNet+Mixup	98.0	97.8
	ChoiceNet	<b>99.1</b>	<b>99.0</b>
80%	ConvNet	90.6	79.0
	ConvNet+Mixup	95.3	95.1
	ChoiceNet	<b>98.3</b>	<b>98.3</b>
90%	ConvNet	76.1	54.1
	ConvNet+Mixup	78.6	42.4
	ChoiceNet	<b>95.9</b>	<b>95.2</b>
95%	ConvNet	50.2	31.3
	ConvNet+Mixup	53.2	26.6
	ChoiceNet	<b>84.5</b>	<b>66.0</b>

Table 8: Test accuracies on the MNIST dataset with randomly permuted label.

Corruption $p$	Configuration	Best	Last
25%	ConvNet	94.4	92.2
	ConvNet+Mixup	97.6	97.6
	ChoiceNet	<b>99.2</b>	<b>99.2</b>
40%	ConvNet	77.9	71.8
	ConvNet+Mixup	84.0	83.0
	ChoiceNet	<b>99.2</b>	<b>98.8</b>
45%	ConvNet	68.0	61.4
	ConvNet+Mixup	68.9	55.8
	ChoiceNet	<b>98.0</b>	<b>97.1</b>
47%	ConvNet	58.2	53.9
	ConvNet+Mixup	60.2	53.4
	ChoiceNet	<b>92.5</b>	<b>86.1</b>

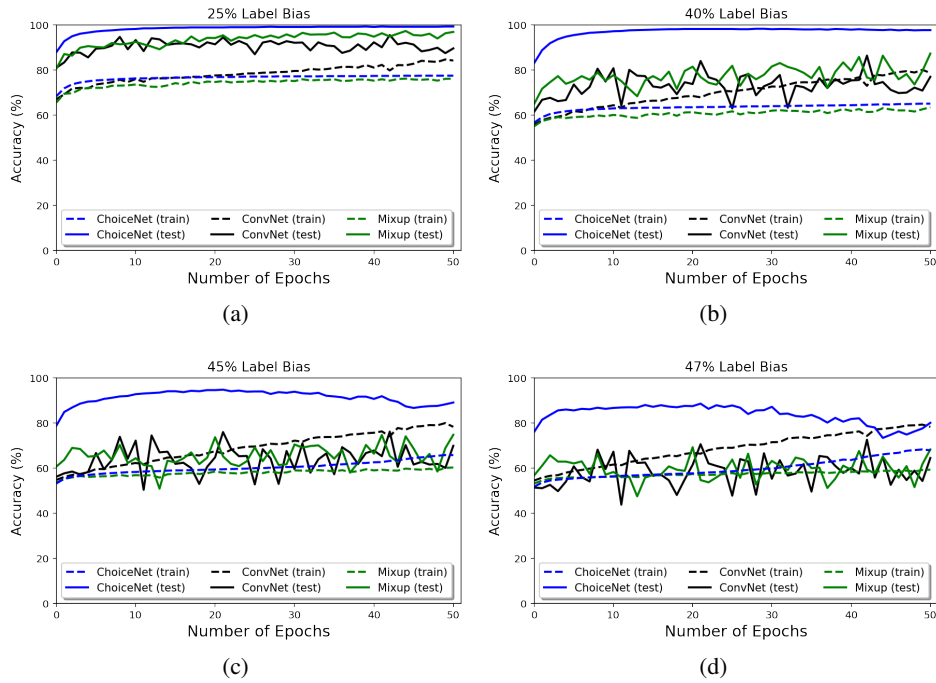


Figure 8: Learning curves of compared methods on random bias experiments using MNIST with different noise levels.

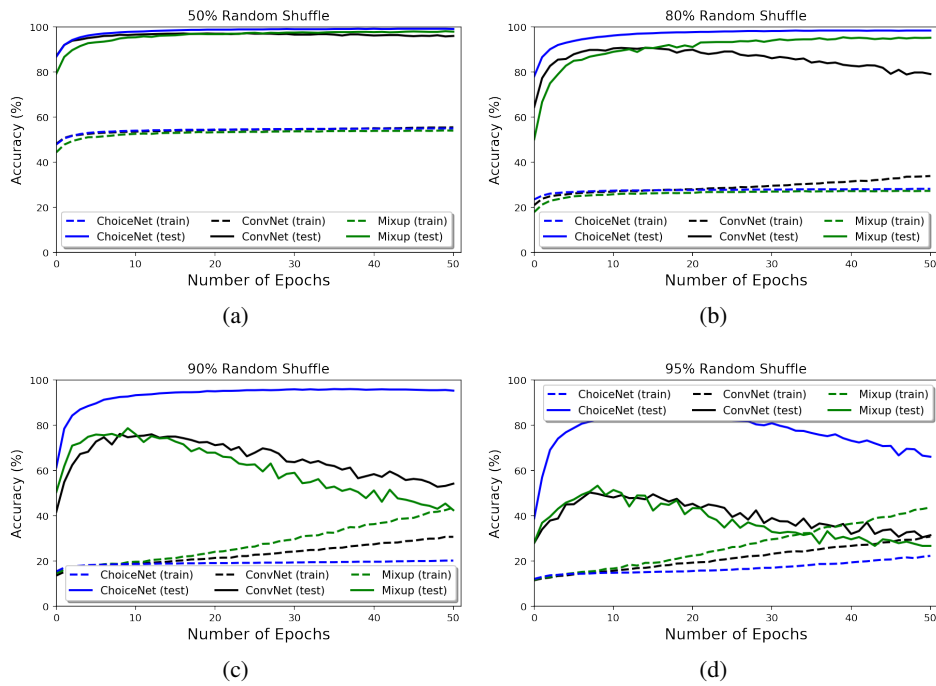


Figure 9: Learning curves of compared methods on random shuffle experiments using MNIST with different noise levels.

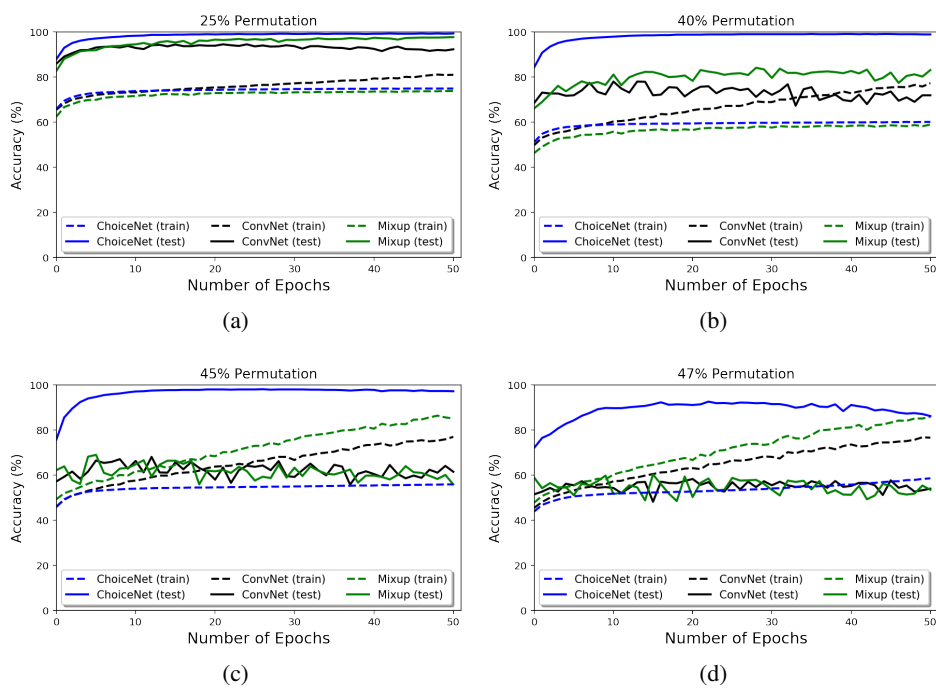


Figure 10: Learning curves of compared methods on random permutation experiments using MNIST with different noise levels.

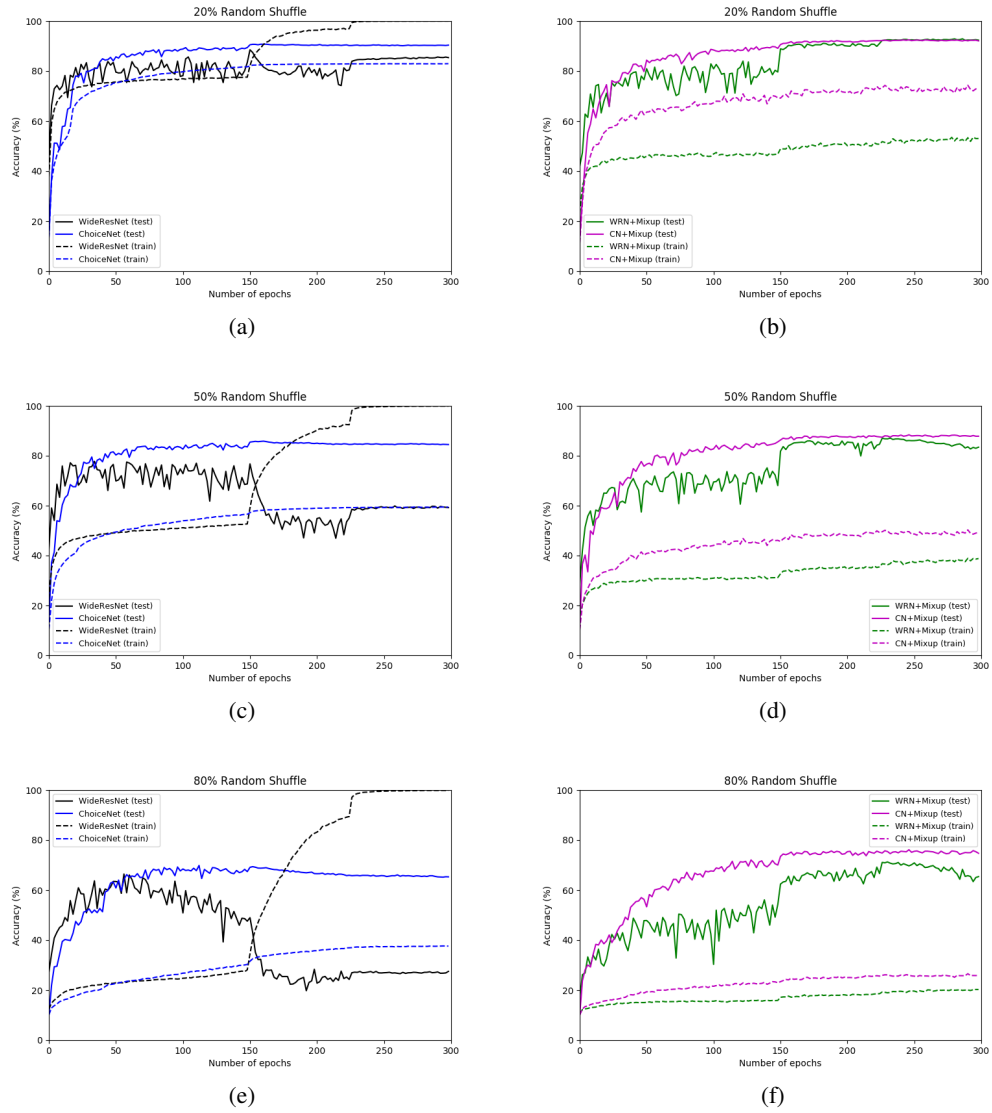


Figure 11: Learning curves of compared methods on CIFAR-10 experiments with different noise levels.